Dissociative Photoionization of 1,3-Dioxolane:

We Need Six Channels to Fit The Elephant

Peter Weidner,[†] Krisztina Voronova,[§] Andras Bodi,[‡] and Bálint Sztáray[†,*]

[†]Department of Chemistry, University of the Pacific, Stockton, CA 95211, USA

[§]Department of Chemistry, University of Nevada, Reno, Reno, NV 89557, USA

[‡]Laboratory for Synchrotron Radiation and Femtochemistry, Paul Scherrer Institute, 5232 Villigen, Switzerland

[*]Corresponding author: bsztaray@pacific.edu.

Abstract

The dissociative photoionization of 1,3-dioxolane was studied by photoelectron photoion coincidence (PEPICO) spectroscopy in the photon energy range of 9.5–13.5 eV. Our statistical thermodynamics model shows that a total of six dissociation channels are involved in the formation of three fragment ions, namely $C_3H_5O_2^+$ (*m/z* 73), $C_2H_5O^+$ (*m/z* 45) and $C_2H_4O^+$ (*m/z* 44), with two channels contributing to the formation of each. By comparing the results of *ab initio* quantum chemical calculations to the experimentally derived appearance energies of the fragment ions, the most likely mechanisms for these unimolecular dissociation reactions are proposed, including a description of the relevant parts of the potential energy surface.

Introduction

Small, oxygen-containing organic molecules play a central role in numerous reactive gas-phase environments (e.g. combustion, atmospheric, and even extra-terrestrial environments). Despite their importance, the study of such environments poses challenges, which can be overcome by the construction of reliable models. These models, however, cannot be more accurate than any of their input parameters. Therefore, models combustion, atmospheric chemistry and extra-terrestrial or interstellar media require accurate thermochemical and kinetic data, which can be obtained using techniques such as photoelectron photoion coincidence (PEPICO) spectroscopy.

1

In our previous works on small, oxygenated molecules, cationic fragmentation patterns were encountered which looked deceptively simple at first glance but turned out to be quite complex in the end. For example, both acetic acid anhydride[1] (almost 50% oxygen by weight) and dimethyl carbonate[2] (more than 50% oxygen by weight) were studied using PEPICO spectroscopy in combination with *ab initio* quantum chemical calculations and statistical modeling.[3] In both cases, the dissociative photoionization mechanism included numerous isomerization steps and even bifurcated reaction pathways. The parallel and sequential dissociative photoionization pathways of the practicable, biomass-derived, liquid transport fuel furfural (only 33% oxygen by weight) were studied by PEPICO and compared with previously established thermal decomposition products.[4] Adipic acid (44% oxygen by weight), a model dicarboxylic acid for secondary organic aerosol components, does not directly result in a parent ion due to poor Franck–Condon overlap, but instead dissociates at the ionization onset.[5] More recently, we applied PEPICO spectroscopy to study the benzylium/tropylium ion dichotomy, and, with the help of careful statistical analysis, we could show that both $C_7H_7^+$ isomer ions are formed from both toluene and cycloheptatriene close to the H-loss threshold.[6] Overall, 1,3-dioxolane, as the simplest stable saturated heterocyclic acetal and containing more than 40% oxygen by mass, fits well into our efforts to map out the ionic fragmentation mechanisms and energetics of oxygen-rich systems. Notwithstanding its simple ring structure and electron ionization mass spectrum, it may still hold the potential for complex multi-step ion fragmentation mechanisms.

First principles trajectory calculations can be used to predict electron ionization mass spectra,[7-8] and a number of a priori algorithms have been proposed to explore potential energy surfaces and identify unimolecular reaction pathways.[9] While *ab initio* mass spectra sometimes show remarkable agreement with experiment,[10] an accurate prediction of the fragment ion masses and their relative intensities does not necessarily validate the underlying mechanism. Furthermore, even the most careful computational studies may miss important reaction channels in the absence of experimental information.[11] Therefore, unveiling the dissociation mechanism of relatively small and simple organic molecules and providing a statistical model to predict rates and branching ratios as a function of internal energy is inherently useful for the development of automated reaction discovery methods.

2

Besides its application in organic synthesis as a polar aprotic solvent, 1,3-dioxolane is used in polymer chemistry and alternative fuel development. 1,3-Dioxolane and its derivatives can serve as monomers in the production of polyether-type polymers through ring opening polymerization under various conditions.[12-15] Furthermore, they are promising biofuel components or fuel additives to improve physical and chemical properties of diesel fuels via intake oxygen enrichment.[16-19] Despite its potential use in alternative fuels – in particular, due to its high oxygen content – accurate and detailed data on the dissociation of 1,3-dioxolane ions is largely absent in recent literature. Electron ionization (EI) mass spectrometric studies on 1,3-dioxolane[20-21] date back more than forty years. At the time, the main fragment ion masses were identified at *m/z* 73, 45, and 44 and a tentative mechanism was proposed for their formation. This mechanism suggests that the *m/z* 73 and *m/z* 44 fragment ions are produced in parallel dissociation reactions via H- and CH_2O-loss respectively, whereas the *m/z* 45 fragment ion is formed in a consecutive CO-loss step from the *m/z* 73 daughter ion. However, EI is too blunt an ionization technique to readily allow for further insights into fragmentation mechanisms, reliable structural assignments, or accurate energetics.

PEPICO spectroscopy, on the other hand, allows for meV-resolution parent ion internal energy selection and, combined with *ab initio* quantum chemical calculations and statistical thermodynamics, can be used to obtain more in-depth information on the dissociative photoionization of 1,3-dioxolane. Similar to other small oxygenated organics (*vide supra*), these dissociation pathways had looked deceptively simple at first, but proved to be far more complex upon closer inspection. Dissociation mechanisms were ultimately elucidated by statistical modeling of the experimental data, indicating multiple competing pathways for the formation of each fragment ion. Stationary points along these pathways were identified using density functional theory (DFT), providing a more complete picture of the dissociative photoionization processes of 1,3-dioxolane.

Methods

Experimental

1,3-Dioxolane (≥99% purity) was purchased from Sigma–Aldrich and used without further purification. The room-temperature sample was seeded through a Teflon tube from the headspace of a glass vial directly into the experimental chamber of the CRF-PEPICO (Combustion

3

Reactions Followed by PEPICO) endstation at the vacuum ultraviolet (VUV) beamline[22] of the Swiss Light Source. Because the sample was introduced effusively, bypassing the quartz flow-tube reactor − the key feature of the CRF-PEPICO setup − only a brief description of the experimental setup is given herein. Detailed information on the CRF-PEPICO apparatus can be found elsewhere.[23]

The experimental chamber pressure was kept at approximately 8×10^{-7} mbar during the experiment, of which less than 2×10^{-7} mbar was the background. The effusively introduced sample was ionized in the ca. 2×2 mm cross-section interaction region by vacuum ultraviolet radiation. Prior to interaction with the sample, the VUV synchrotron radiation was collimated, dispersed in grazing incidence by a 150 grooves/mm blazed grating, and focused at the exit slit in a differentially pumped gas filter at a resolution of 5−8 meV at threshold. Higher harmonics were suppressed by the gas filter filled with Ne–Ar–Kr mixture at 10 mbar pressure. The photon energy was calibrated using Ar 11s'−14s' autoionization lines at the first and second orders of the grating.

Photoelectrons and photoions were extracted in opposite directions from the interaction region by a constant 125 V cm^{-1} electric field. Photoelectrons, which provide the start signal in the multiple-start/multiple-stop coincidence acquisition scheme,[24] were kinetic energy analyzed with sub-meV resolution at threshold using velocity map imaging (VMI) on a Roentdek DLD40 position sensitive delay-line detector mounted 750 mm from the ionization point. Zero kinetic energy (threshold) electrons are detected in the center of the image, together with those non-zero kinetic energy ("hot") electrons that have no off-axis momentum component. In order to obtain coincidences with only true threshold electrons, the hot electron contamination can be eliminated by subtracting the product of an experimentally determined (detector area ratio) factor and the coincidence spectrum corresponding to a ring area around the central spot from the center signal.[25] The ions were mass analyzed by a two-stage Wiley–McLaren TOF mass spectrometer[26] with a 2.7 cm long extraction, an 8.7 cm long acceleration and an 88.6 cm long field free drift region, and detected by a Roentdek DLD40 microchannel plate detector. The length of the extraction region combined with the applied 125 V cm^{-1} extraction field provides ion residence times in the order of microseconds. Under these conditions, metastable parent ions with unimolecular dissociation rates between 10^3–10^7 s^{-1} yield asymmetric fragment ion peaks in the

4

TOF mass spectra.[3] Such peaks were not observed during our measurements, indicating that only fast dissociations occurred. Although we could detect no asymmetry or peak shift in the hydrogen-loss daughter ion ($C_3H_5O_2^+$, m/z 73) peak, either, the low extraction field limited the mass resolution, which was insufficient for baseline separation of the molecular ion ($C_3H_6O_2^+$, m/z 74) and the m/z 73 peak, as shown in **Figure S1** in the Supporting Information (SI). In order to determine the fractional abundances of these ions, a center-of-gravity deconvolution process was applied.[27-28] The center of gravity (CoG) for these TOF bands can be calculated according to

$$\mu = \frac{\int t\, I_{\text{TOF}}(t)\mathrm{d}t}{\int I_{\text{TOF}}(t)\mathrm{d}t}$$

where μ is the CoG of the combined peaks (m/z 73 and 74) from the hot electron-subtracted time-of-flight spectrum, $I_{\text{TOF}}(t)$. The contributions of the parent and daughter ions (a and $[1-a]$, respectively, where $0 \leq a \leq 1$) can be calculated from the following equation:

$$\mu = at_1 + (1-a)\,t_2$$

where t_1 and t_2 are arrival times of the $C_3H_6O_2^+$ (m/z 74) and $C_3H_5O_2^+$ (m/z 73) ions, respectively.

Computational

The Gaussian 09 suite of programs[29] was used for *ab initio* quantum chemical calculations to provide further insight on the dissociative photoionization mechanism of 1,3-dioxolane, including input for the statistical model. Reaction paths and transition state (TS) structures were located by constrained optimizations and by the synchronous transit-guided quasi-Newton (STQN) method.[30-31] Vibrational frequencies and rotational constants were calculated at the B3LYP/6-311++G(p,d) level of theory[32-33] and were used to obtain a thermal energy distribution of the neutral precursor molecule, densities and numbers of states in the rate equation (*vide infra*), and the internal energy distribution of the intermediate fragments based on a statistical distribution of product internal energies.[34] In order to verify the reaction mechanisms, intrinsic reaction coordinate (IRC) calculations[35] were carried out starting from the located transition states. Minima in both the forward and reverse directions were reoptimized to confirm the lowest energy structures on both the reactant and product sides. Local minima and saddle points that most likely play a role in the dissociative photoionization process were evaluated using the higher level G4 composite method.[36] Finally, the ionization energy (IE) of 1,3-dioxolane was calculated using

5

CBS-QB3, W1U, G3 and G4 composite methods and an average value was used in the statistical model.[36-39]

Statistical Modeling

The question whether the ergodic hypothesis holds and the dissociation is governed by statistical theory is all the more pertinent when the breakdown curves exhibit unusual trends, as is certainly the case for 1,3-dioxolane (see below). In non-statistical dissociations, a nuclear[40] or an electronic[41-42] degree of freedom is decoupled from the rest, which may markedly change the dissociation kinetics and the resulting internal energy distributions.[43] Rate constants for non-statistical channels may increase significantly and statistically minor channels may become dominant. However, as we will show, the competition between the six dissociation channels of dioxalane ions is near-perfectly described by statistical rate theory in the studied energy window. Therefore, the dissociative photoionization of 1,3-dioxolane passes the "duck test of statisticality" [44] and the fragmentation process takes place on the bound ground electronic state of the cation.

The unimolecular rate constant, $k(E)$, for each dissociation pathway at internal energy, E, can be calculated using Rice–Ramsperger–Kassel–Marcus (RRKM) theory,[45-47] as coded in our modeling tool:[3]

$$k(E) = \frac{\sigma N^{\ddagger}(E - E_0)}{h\rho(E)},$$

where $N^{\ddagger}(E - E_0)$ is the number of states of the transition state at given excess energy (E) above the threshold at E_0, $\rho(E)$ is the density of states of the molecule, h is Planck's constant, and σ is the symmetry number of the reaction. The densities and sums of states were calculated using harmonic vibrational frequencies by the Beyer–Swinehart direct count algorithm.[48] Fractional ion abundances were modeled as a function of photon energy to obtain the breakdown diagram (solid lines, **Figure 1**). Experimental appearance energies were obtained from the statistical model, in which the calculated transitional frequencies of the transition states were scaled with a factor and the appearance energies were varied to fit the model to the experimental data.

6
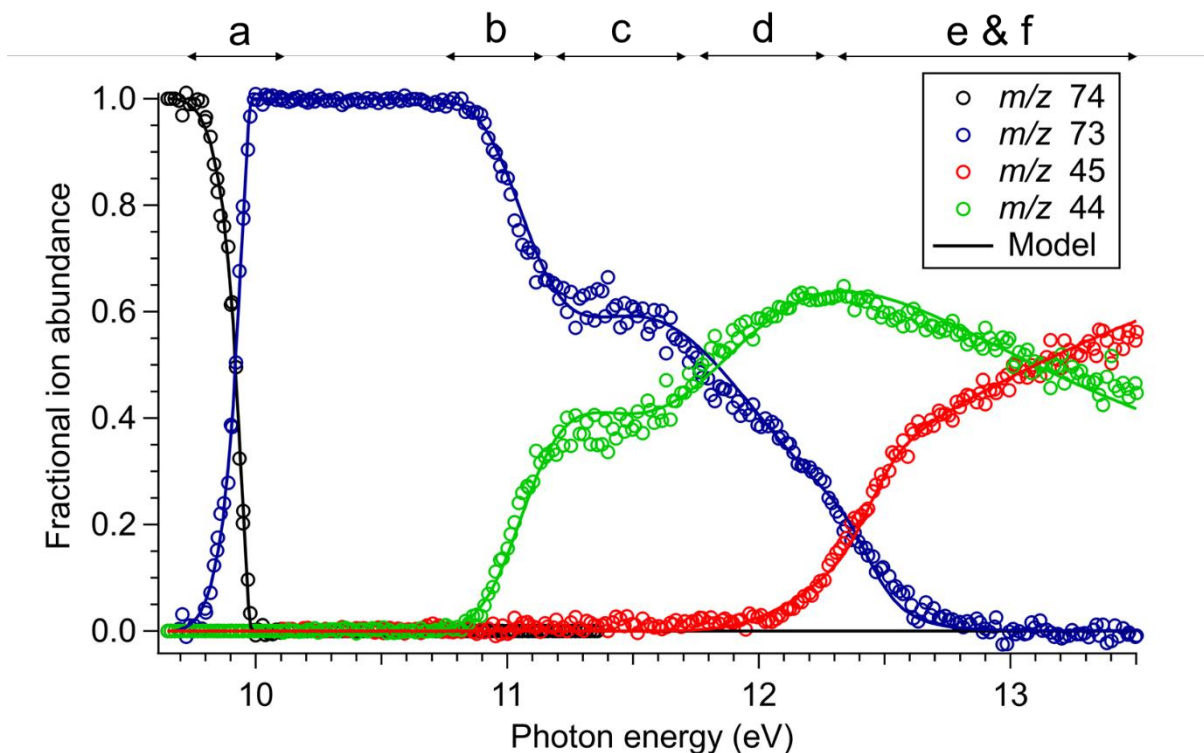
Figure 1. Breakdown diagram of 1,3-dioxolane showing different regions corresponding to the identified dissociation channels (a-f). Empty circles show the experimental data points and solid lines correspond to the results from the statistical model.

Results and Discussion

Dissociative photoionization processes

Threshold photoionization time-of-flight mass spectra were recorded to examine the dissociative photoionization of 1,3-dioxolane. This process yields fragment ions with three different m/z values in the photon energy range of 9.5–13.5 eV, namely $C_3H_5O_2^+$ (m/z 73), $C_2H_5O^+$ (m/z 45) and $C_2H_4O^+$ (m/z 44), in agreement with previous mass spectrometric studies on 1,3-dioxolane.[20-21] The m/z 73 fragment ion is the product of a hydrogen atom loss from the molecular ion (**Figure 2**, reactions a and c), whereas the m/z 45 fragment may originate either from the molecular ion by formyl radical loss (**Figure 2**, reaction e), or from the H-loss daughter ion by a consecutive loss of carbon monoxide (**Figure 2**, reaction f). Similarly, there are two possible sources of the m/z 44 fragment ion as well; it can be produced either in a parallel fashion by the loss of formaldehyde from the molecular ion (**Figure 2**, reactions b and d) or consecutively, by formyl radical loss

7

from the *m/z* 73 fragment (not pictured in **Figure 2**, because ruled out as a contributor, *vide infra*).
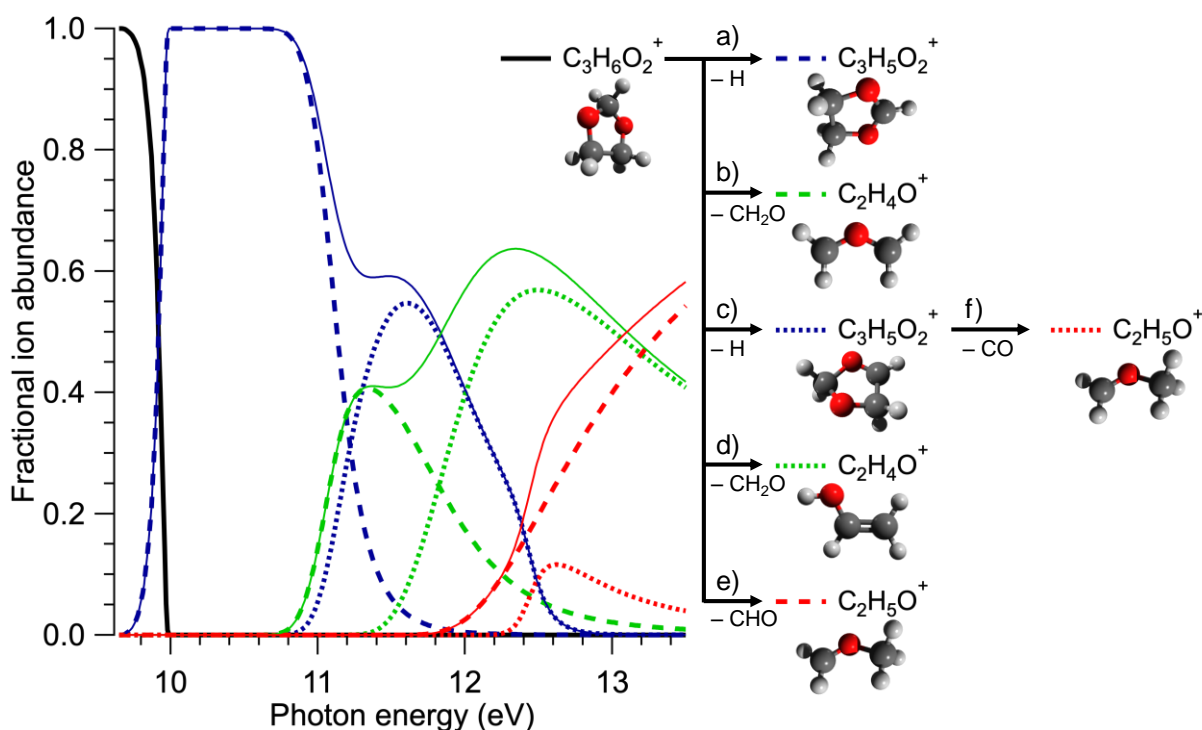
Figure 2. Statistical model of the breakdown diagram (left) and the dissociation channels (a-f) (right). Dashed lines represent the contribution of individual dissociation channels and solid lines correspond to the summed contribution of fragment ions with the same *m/z* values. (Numbering of the dissociation channels corresponds to the regions in Figure 1; structures obtained from quantum chemical calculations, see text).

Visual inspection of the overall appearance of the breakdown diagram (**Figure 1**) can already yield significant insights into the dissociation mechanism.[1, 3-4, 49] The first dissociation channel, the loss of a hydrogen atom from the molecular ion, yields the *m/z* 73 fragment ion with an appearance energy of ≈10.0 eV (**Figure 1**, region a; **Figure 2**, blue line). This ion is the only detected fragment up to approximately 10.9 eV photon energy, where the second daughter ion (*m/z* 44) appears (**Figure 1**, region b; **Figure 2**, green line). The initial steep rise in the fractional abundance of this fragment (and the corresponding steep fall-off of the H-loss ion) indicates either a consecutive dissociation from the *m/z* 73 daughter ion, or a parallel dissociation with a significantly looser transition state than the TS of the first dissociation channel. In the photon energy range of 11.2–11.6 eV (**Figure 1**, region c), a rather peculiar feature can be observed in

8

the breakdown diagram, namely the abrupt and transient plateauing of the fractional ion abundances of the *m/z* 73 and 44 fragment ions. This suggests that a second channel is likely to open here, producing the *m/z* 73 fragment ion through a new mechanism (**Figure 2**, dotted blue line) and thereby compensating for the decline in the fractional abundance of this ion. Starting from approximately 11.7 eV, the fractional abundance of the *m/z* 44 ion starts to increase again (**Figure 1**, region d), hinting at a second pathway for this fragment ion opening up (**Figure 2**, dotted green line). Based on the shape of the curves between 11.7 and 12.1 eV, this dissociation process is most likely in parallel with the H-loss dissociation channels. The highest energy fragment detected in our experiment (*m/z* 45) appears above 12.0 eV. Again, the breakdown curve corresponding to this fragment ion can be clearly divided into two separate regions with different slopes (*i.e.* a steeper slope up to ≈12.6 eV followed by a gentler slope until the end of the photon energy range of our measurement, **Figure 1**, regions e and f; **Figure 2**, red lines). This feature suggests that there are multiple reactions involved in the formation of the *m/z* 45 daughter ion.

Modeling of the breakdown diagram

Reaction rates and energy distributions were modeled using statistical thermodynamics (RRKM theory, *vide supra*) in order to extract accurate photoionization onsets from the experimental PEPICO data. While in general it is preferred to rely on well-established experimental IEs, such are only available if the original transition is observable and the photoelectron spectrum can be assigned.[5] In the light of our calculations, the 1,3-dioxolane ionization energies reported by Collin and Conde,[50] and Sweigart and Turner[51] are clearly overestimated at 10.02 and 9.9 eV, respectively. In the model, an adiabatic ionization energy (IE) of 9.81 eV was used, as obtained from quantum chemical calculations, by averaging the IEs at the CBS-QB3, W1U, G3 and G4 composite levels (providing calculated ionization energy values of 9.82, 9.82, 9.80 and 9.79 eV respectively). A relaxed sample temperature of 280 K provided the best fit to the measured data, which is not too far from the experimental temperature of 300 K and may indicate some expansive cooling.

The typical modeling approach for a system with a nontrivial fragmentation mechanism consists of multiple steps. First, a cursory inspection of the breakdown diagram is used to determine

9

parallel and sequential dissociation channels, based on the steepness of the breakdown curves and their correlation, *vide supra*.[5, 52] Then, approximate threshold energies are obtained and used to guide *ab initio* calculations to explore the part of the potential energy surface (PES) governing the fragmentation processes. These precursor ions and transition states then provide the starting point for the statistical model, the third step, which is fitted to the breakdown diagram (and, if measured, the rate curves) to obtain quantitative energetics data. Finally, previously calculated stationary points of the PES are refined and further calculations are carried out in order to find the most likely mechanisms which are in best agreement with the experimental data.

A cursory inspection of the dioxolane breakdown diagram, however, raises more questions than it answers. Based on the shape of the breakdown curves above the first dissociation process, *i.e.,* above 10.5 eV (**Figure 1**, regions b–f), it appears likely that more than one channel contributes to the formation of each fragment ion in a significant way. Because of the complexity of the dissociative ionization mechanism, statistical modeling and the *ab initio* exploration of the potential energy surface are used hand-in-hand to provide a self-consistent picture of the fragmentation reactions, as outlined below.

To start, the experimental breakdown curves were fitted up to 11 eV photon energy (**Figure 1**, regions a and b), only including the first two dissociation channels, producing the *m/z* 73 and *m/z* 44 fragment ions. The first channel was modeled as a single H-loss from the molecular ion and the best fit of the model provided an experimental appearance energy of 9.99 ± 0.02 eV. As a hydrogen loss always carries the possibility of tunneling, this channel was modeled considering this option as well. In this latter case the model shows that the H atom tunnels through a barrier at 10.14 ± 0.02 eV with the reverse barrier height and critical frequency determined computationally.[53-54] A cursory visual inspection of the second dissociation channel (**Figure 1**, region b) suggests a consecutive process, because the *m/z* 44 signal rises quite rapidly. However, when this channel is handled as a consecutive formyl-radical loss from the first fragment ion (*m/z* 73), the modeled curve is much too steep (see **Figure S2** in SI). Overall, the inflection points, a plateau, and a sloping maximum in the *m/z* 44 breakdown curve reminded us more of the contours of an elephant devoured by a boa constrictor[55] than of a typical consecutive dissociation process. Furthermore, calculations suggest that sequential formyl loss is energetically forbidden below a photon energy of ≈13.5 eV (**Table S1** in SI). Consequently, we conclude that the *m/z* 44

10

fragment ion is formed directly from the molecular ion, for which several energetically allowed pathways are also found (*vide infra*). Reassuringly, when modeled as formaldehyde loss from the molecular ion, in parallel with the H-loss channel, the model breakdown curve for the *m/z* 44 ion is in good agreement with the experimental data. The experimental 0 K appearance energy for the *m/z* 44 fragment was thus determined to be 10.81 ± 0.05 eV.

Next, the fractional ion abundances were calculated up to 12 eV photon energy, including the plateauing and crossing region (**Figure 1**, regions c and d), but not including the appearance of the highest energy fragment ion *m/z* 45. The famous quote *"With four parameters I can fit an elephant and with five, I can make him wiggle his trunk,"* attributed to John von Neumann (Hungarian: Neumann János Lajos) immediately comes to mind.[56] Indeed, we intended to model this region of the breakdown curves with the fewest possible dissociation channels, to avoid over-parametrization. This was achieved using a step-by-step approach, in which we only included an additional channel in the model if the breakdown diagram could not be faithfully reproduced without that channel taken into account. To begin, an additional parallel dissociation channel was included for *m/z* 73 fragment ion (**Figure 2**, dotted blue line), which was suggested by the abruptly appearing plateau between 11.2 and 11.5 eV (**Figure 1**, region c). While including this channel took care of the plateau region, at higher photon energies, the model deviated from the experimental data significantly (**Figure S3**, a), indicating the presence of at least one additional dissociation channel here. Modeling this channel as a consecutive dissociation from the H-loss product does not result in an acceptable fit (**Figure S3**, b) and quantum chemical calculations also rule out the formation of the *m/z* 44 ion from the H-loss product (*vide supra*). Therefore, a second parallel dissociation channel, forming the *m/z* 44 fragment ion, was added (**Figure 2**, dotted green line). This expanded model provides a reasonably good fit to the experimental data up to approximately 12 eV (**Figure 1**, regions a-d) and the resulting best-fit appearance energies are 10.90 ± 0.08 eV and 11.30 ± 0.06 eV for the second *m/z* 73 and 44 channels, respectively.

Finally, the highest energy fragment, *m/z* 45, up to 13.5 eV photon energy was included in the model (**Figure 1**, regions e and f). Again, the shape of this breakdown curve indicates that there are at least two different dissociation channels involved in the formation of this fragment ion. The best fit was achieved by considering both a parallel (from the molecular ion) and a consecutive (from *m/z* 73) channel to form the *m/z* 45 fragment ion (the dashed and dotted red lines in **Figure**

11

2, respectively), with experimental appearance onsets of 11.62 ± 0.06 eV and 12.39 ± 0.09 eV, respectively. With a total of six channels (two for each detected fragment ion; see **Figure 2**) included in the model, a very good fit to the experimental data was achieved, as shown in **Figure 1**. While five parallel dissociation channels in a PEPICO experiment have been modeled already,[52] this is the first time that a dissociative photoionization mechanism could be revealed and quantitatively modeled with six processes based on the mass spectral signal of only three fragment ions. Finally, let us emphasize it once more that models with fewer dissociation channels did not provide an even qualitatively acceptable fit.

Potential energy surface

By statistical rate modeling of the experimental breakdown diagram, a total of six dissociation channels were identified, including two parallel channels forming the *m/z* 73 fragment ion through a H-loss from the molecular ion of 1,3-dioxolane (**Figure 2**, blue lines, channels a and c), two parallel channels forming the *m/z* 44 fragment ion by CH_2O-loss from the *m/z* 74 parent ion (**Figure 2**, green lines, channels b and d), and both parallel and consecutive channels forming the *m/z* 45 fragment ion through formyl radical loss from the molecular ion or through CO-loss from the H-loss fragment ion, respectively (**Figure 2**, red lines, channels e and f). In order to gain further insight into the mechanisms of these dissociation reactions, density functional theory was employed at the B3LYP/6-311++G(d,p) level to explore the potential energy surface driving the fragmentation of the parent ion. Transition states were located by scanning along the internal coordinates or by using STQN calculations. The energies of the stationary points of interest were refined by the G4 composite method. Reported below are the 0 K G4 energies relative to the neutral molecule of 1,3-dioxolane. Even though a significant portion of the potential energy surface was explored, only those mechanisms are described in detail which contributed to our understanding of the dissociative photoionization mechanism.

Formation of the *m/z* 73 fragment ion. Based on the breakdown diagram, two channels are involved in the hydrogen atom loss from the *m/z* 74 molecular ion, resulting in the formation of the *m/z* 73 fragment ion, as summarized in **Figure 3**. There are two possibilities for H-loss through direct bond cleavage from the molecular ion [**1**]. Dissociation of a H-atom from the acetal position (**Figure 2**, channel a) involves a transition state [**2**]‡ at 10.123 eV energy and

12

results in the formation of the H-loss fragment ion [**3**]. This calculated energy is in very good agreement with the experimentally derived 10.14 ± 0.02 eV appearance energy which was obtained by modeling this channel including tunneling through the *ab initio* calculated Eckart barrier.[53-54] Alternatively, a hydrogen atom can be lost from a non-acetal carbon (**Figure 2**, channel c). In this case, scanning along the C–H bond does not indicate a saddle point, which is why the transition state is looser than in the first case, the rate curve is steeper, and the channel quickly becomes competitive with increasing energy. The calculated thermochemical limit for the formation of the second H-loss fragment ion [**4**] is in good agreement with the experimentally derived onset of this channel (calculated: 10.847 eV; experimental: 10.90 ± 0.08 eV).
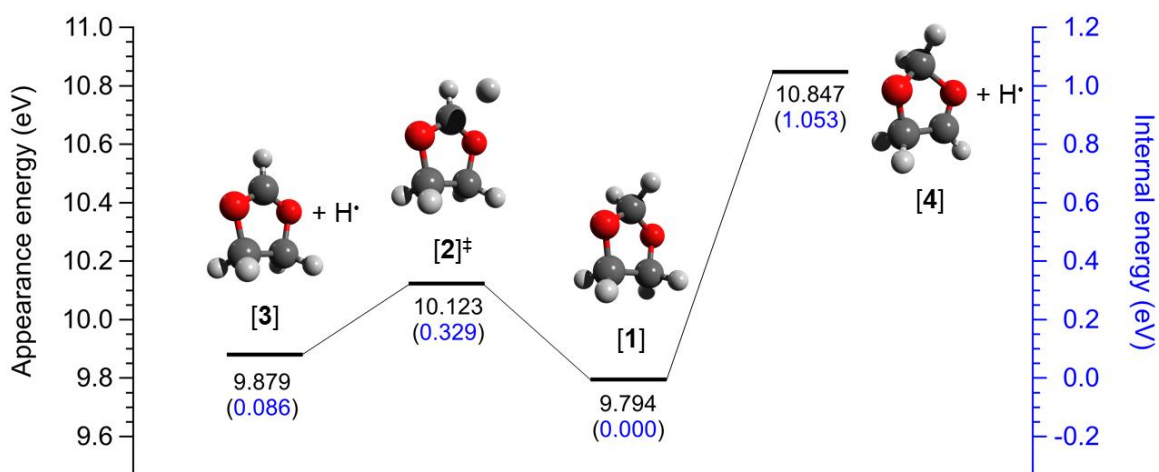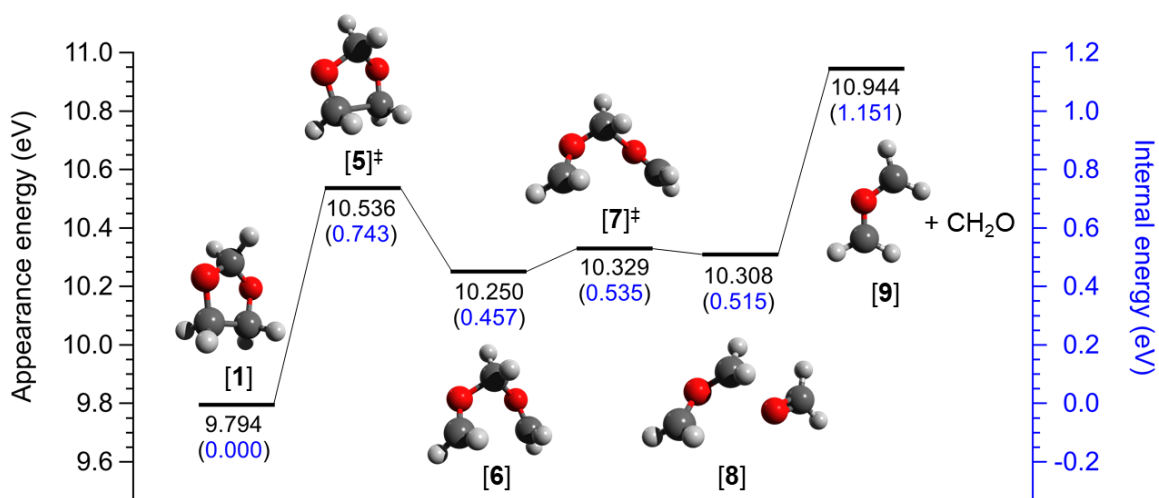

Figure 3. Formation of the *m/z* 73 fragment ion (channels a and c). The 0 K G4 appearance and internal energies are reported relative to the neutral 1,3-dioxolane molecule and the molecular ion respectively.

Formation of the *m/z* 44 fragment ion. An *ab initio* theoretical study by Bouma et al. examined the stabilities of eleven different isomers of *m/z* 44 fragment ions with the elemental composition of $C_2H_4O^+$ and concluded that, besides three well-established isomers (molecular ions of vinyl alcohol, acetaldehyde and oxirane), there is a fourth stable isomer with relatively low energy, $CH_2OCH_2^{+}$.[57] The experimental evidence for the formation of this fourth low energy $C_2H_4O^+$ isomer was provided a few years after the theoretical study by Baumann and MacLeod.[58] Based on this information, all four of the above mentioned isomers were considered as possible

13

structures for the *m/z* 44 fragment ion detected in the dissociative photoionization of 1,3-dioxolane. When formed together with the neutral CH_2O fragment from the molecular ion, the G4-calculated thermochemical limits for the formation of all four isomers (9.800–11.868 eV; **Table S1**) are around or under the experimentally derived appearance energies (10.81 ± 0.05 and 11.30 ± 0.06 eV). In contrast, thermochemical limits for the formation of the *m/z* 44 fragment ion by sequential H- and CHO-losses (13.560–15.627 eV; **Table S1**), are several eV higher that the experimentally derived appearance energies and can thus clearly be excluded. This is in agreement with our modeling work as well, which also suggested that the *m/z* 44 fragment ion is formed in parallel processes.

Upon further investigation, the number of possible $C_2H_4O^+$ isomers can be narrowed down to two. According to previous studies, both acetaldehyde and oxirane exhibit further dissociations in the energy range of the breakdown diagram.[59-61] However, we have not detected the corresponding fragment ions in the 1,3-dioxolane experiments, which rules out the involvement of these $C_2H_4O^+$ isomers as intermediate fragment ions. Therefore $CH_2OCH_2^+$ [**9**] and the vinyl alcohol cation are possible dioxolane fragment ions and these were considered in the proposed dissociation mechanisms, discussed in detail below.

Figure 4. Formation of the *m/z* 44 fragment ion initiated by ring-opening (channel b). The 0 K G4 appearance and internal energies are reported relative to the neutral 1,3-dioxolane molecule and the molecular ion respectively.

14

The pathway with the lowest energy barrier (**Figure 2**, channel b; **Figure 4**) includes two bond cleavage steps and eventually results in the formation of $CH_2OCH_2^+$ fragment ions. The first step of this mechanism is the ring opening of the molecular ion [**1**] through C–C bond cleavage with a barrier at 10.536 eV (TS [**5**]‡). The open chain isomer [**6**] of the molecular ion already contains a formaldehyde moiety at terminal position. The next step of the dissociation is a C–O bond cleavage, including a transition state [**7**]‡ at 10.329 eV and resulting in the formation of an ion–neutral complex of $CH_2OCH_2^+$ fragment ion and formaldehyde [**8**]. This complex can dissociate at 10.944 eV, the thermochemical limit for the formation of separate $CH_2OCH_2^+$ [**9**] and formaldehyde. As the energy for this dissociation process is higher than any previous barrier involved in this mechanism, the submerged transition states will not affect the energy requirement of this reaction and, therefore, the highest barrier will be equal to the thermochemical limit. The calculated thermochemical limit of 10.944 eV is in reasonable agreement with the experimentally derived 10.81 ± 0.05 eV.
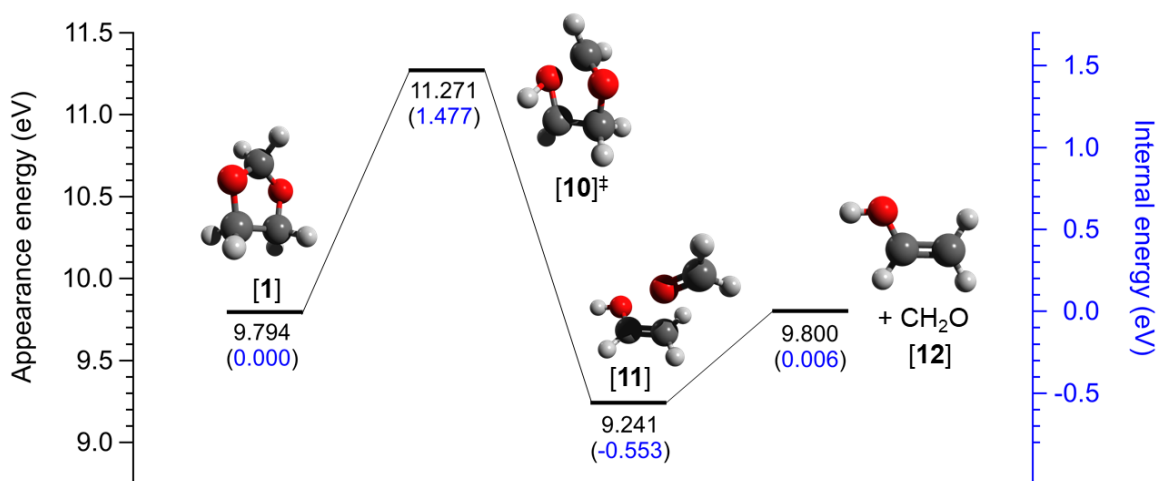
Figure 5. Formation of the *m/z* 44 fragment ion initiated by hydrogen-shift (channel d). The 0 K G4 appearance and internal energies are reported relative to the neutral 1,3-dioxolane molecule and the molecular ion respectively.

The second channel producing the *m/z* 44 fragment ion (**Figure 2**, channel d; **Figure 5**) involves multiple bond cleavages as well and is initiated by a hydrogen shift between one of the non-acetal position carbon atoms and an adjacent oxygen atom of the molecular ion of 1,3-dioxolane [**1**]. The transition state [**10**]‡ associated with this H-shift has a calculated energy of 11.271 eV, which

15

is in excellent agreement with the experimentally derived onset of this channel, 11.30 ± 0.06 eV. After overcoming this barrier, an ion–neutral complex [**11**] of ionized vinyl alcohol and formaldehyde is formed. This complex, however, has a high enough excess energy to immediately dissociate into its components – the vinyl alcohol cation [**12**] and formaldehyde.

Formation of the *m/z* 45 fragment ion. Four distinct structures were considered as the most likely isomers for the *m/z* 45 fragment ion. These structures are protonated vinyl alcohol, protonated acetaldehyde, protonated oxirane and $CH_3OCH_2^+$, all of which can be regarded as H-adducts of the analogous *m/z* 44 structures (*vide supra)*. The thermochemical limits of all four possible *m/z* 45 isomers were calculated for two different reactions: formyl radical loss from the molecular ion and CO-loss from the H-loss fragment ion. In case of the former, calculated values are in the range of 9.583–10.792 eV, whereas for the consecutive CO-loss, calculated thermochemical limits are between 10.202–11.412 eV (**Table S1**). Consequently, both paths were considered as possible ways of forming the *m/z* 45 fragment ions. The experimentally derived appearance energies of both of these reactions are above all calculated thermochemical limits at 11.62 ± 0.06 eV and 12.39 ± 0.09 eV, respectively. The most likely mechanisms of these reactions are described below and summarized in **Figure 6** and **Figure 7**.

Formyl radical loss from the molecular ion starts with a ring opening step followed by a hydrogen shift (**Figure 2**, channel e; **Figure 6**). The molecular ion [**1**] can open up at 10.510 eV to form the open chain isomer [**13**] in a process without a reverse barrier. A hydrogen shift between two terminal carbon atoms of open chain isomer [**13**] leads to the formation of a loosely bonded ion-neutral complex of $CH_3OCH_2^+$ ion and formyl radical [**15**]. As the formation of complex [**15**] involves a transition state [**14**]‡ with 11.343 eV relative energy, complex [**15**] has enough excess energy to immediately dissociate into its components, $CH_3OCH_2^+$ ion [**16**] and formyl radical, thus forming *m/z* 45 fragment ion in a parallel fashion. The highest calculated barrier of 11.343 eV of this reaction is in acceptable agreement with the experimentally derived 11.62 ± 0.06 eV, therefore the above described mechanism is regarded as a plausible way of forming the *m/z* 45 fragment ion, but the exact transition state cannot be located with certainty. Furthermore, the calculated transition state is significantly tighter than the best fit in the statistical model, which indicates that while the calculated pathway is of lower energy, a higher-lying route with a looser transition state may be kinetically favored.

16
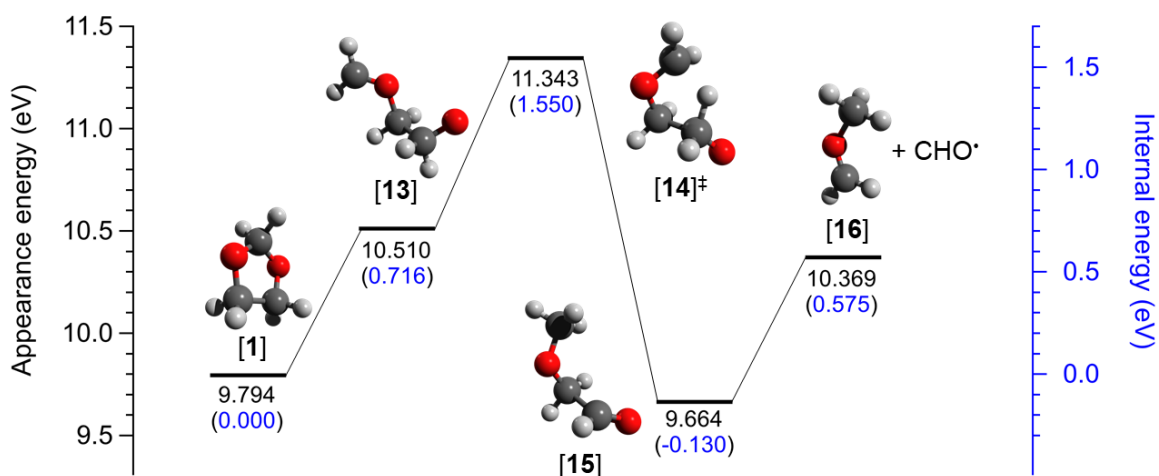
Figure 6. Formation of the *m/z* 45 fragment ion in a parallel fashion (channel e). The 0 K G4 appearance and internal energies are reported relative to the neutral 1,3-dioxolane molecule and the molecular ion respectively.

The second reaction forming the *m/z* 45 fragment ion is a consecutive CO-loss from the H-loss fragment ion (**Figure 2**, channel f, **Figure 7**). Our model shows that the precursor for this reaction must be the H-loss fragment ion [**4**], as the channel forming the first H-loss fragment ion [**3**] (**Figure 2**, channel a) is completely overcome by the second H-loss channel (**Figure 2**, channel c) in the photon energy range where the *m/z* 45 fragment ion appears (**Figure 1**). Furthermore, the isomerization barrier between [**3**] and [**4**] was located at 13.488 eV, further supporting that [**3**] can be excluded as the precursor of the *m/z* 45 fragment ion in the energy range of our experiment. CO-loss from the H-loss fragment occurs through a five membered H-shift transition state [**19**]‡, similar to the one involved in the previous channel (channel e, [**14**]‡). The formation of TS [**19**]‡ is preceded by a rotational isomerization step (TS [**17**]‡: 11.569 eV; rotamer [**18**]: 11.564 eV), and eventually results in the formation of a local minimum [**20**] at 10.999 eV, which can easily lose CO through TS [**21**]‡ (11.070 eV) forming $CH_3OCH_2^+$ (*m/z* 45, [**16**]). The calculated barrier for this reaction (12.088 eV) is in acceptable agreement with our experimentally derived onset of the consecutive CO-loss channel at 12.39 ± 0.09 eV.
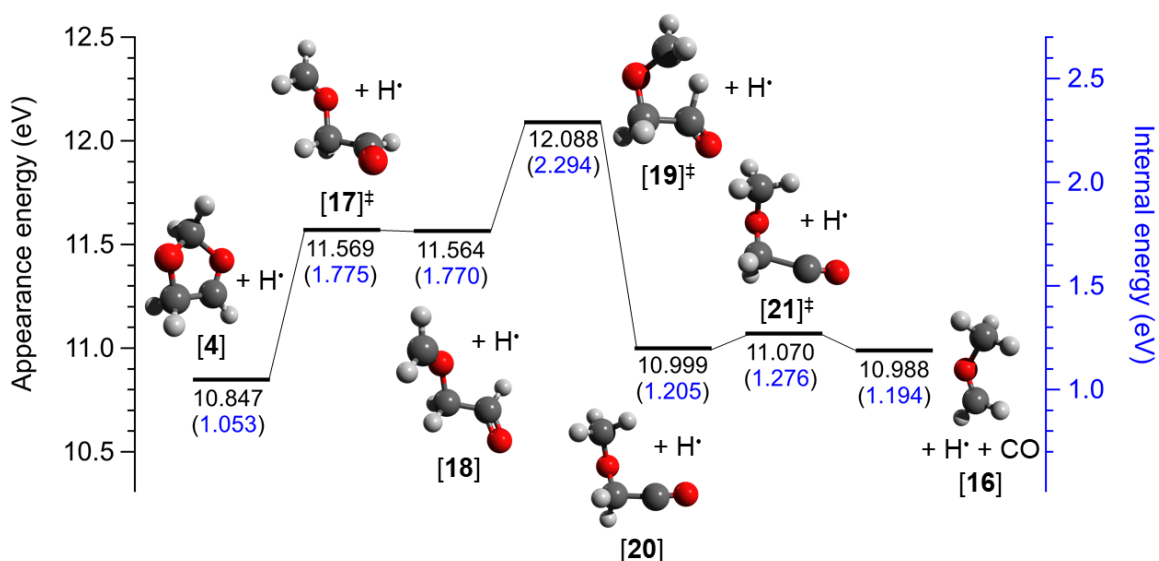
Figure 7. Formation of the *m/z* 45 fragment ion in a consecutive fashion (channel f). The 0 K G4 appearance and internal energies are reported relative to the neutral 1,3-dioxolane molecule and the molecular ion respectively.

Conclusions

Dissociative photoionization of the smallest stable cyclic acetal 1,3-dioxolane was studied by PEPICO spectroscopy. Combining this experimental technique with *ab initio* quantum chemical calculations and statistical rate modeling, the dissociation channels involved in this process were identified alongside with the likely structures and energies of the stationary points driving the dissociative photoionization on the potential energy surface. Similar to other small oxygenated organics previously studied by PEPICO spectroscopy, a more complex dissociation mechanism was uncovered than initially anticipated, based on available literature and the number of detected fragment ions ($C_3H_5O_2^+$, *m/z* 73; $C_2H_5O^+$, *m/z* 45; $C_2H_4O^+$, *m/z* 44). Our model unveiled significant complexity, as two channels were required to model the formation of each fragment ion and fit the breakdown diagram. Fewer channels could not even qualitatively reproduce the experimental data, showing that the final model did not suffer from over-parametrization.

The most likely pathways for the six dissociation channels involved in the dissociative photoionization of 1,3-dioxolane were revealed. These include two channels forming the H-loss fragment ion (with experimental appearance energies of 10.14 ± 0.02 and 10.90 ± 0.08 eV respectively), corresponding to hydrogen losses from either the acetal or one of the non-acetal

18

carbon atoms of the molecular ion of 1,3-dioxolane. The latter step is a barrierless dissociation, whereas the former one includes a tight transition state structure. Modeling this step indicates that the hydrogen tunnels through this barrier when lost from the acetal position. Two channels result in the formation of the m/z 44 fragment ion, which are both direct CH_2O-losses from the molecular ion (experimental appearance energies: 10.81 ± 0.05 and 11.30 ± 0.06 eV). The lower energy channel proceeds through a ring opening mechanism and produces $CH_2OCH_2^+$ as the m/z 44 fragment ion. Although transition state structures were identified along this dissociation pathway, the highest energy barrier is actually the thermochemical limit of the formation of $CH_2OCH_2^+$ and CH_2O. The higher energy reaction forming the m/z 44 fragment ion is initiated by a H-shift between a non-acetal carbon and an adjacent oxygen atom of the molecular ion and produces ionized vinyl alcohol. Finally, the highest energy fragment ion, m/z 45 is formed through a parallel and a consecutive dissociation step. These two mechanisms are similar, as both include rotational isomerization of the precursor ions and H-shifts to form the final products ($CH_2OCH_3^+$ ion and either $CHO^\bullet$ or CO). The parallel channel was identified as a formyl radical loss from the molecular ion (experimental appearance energy: 11.62 ± 0.06 eV), whereas the consecutive channel is most likely a CO-loss from the higher energy H-loss daughter ion (experimental appearance energy: 12.39 ± 0.09 eV). For both of these reactions, the theoretical estimates for the transition states are somewhat lower than the experimental values, which may indicate that other, potentially higher but less tight, saddle points may also play a role in these dissociations.

While the dissociative photoionization of 1,3-dioxolane turned out to be more complex than initially assumed based on the low number of fragment ions, it provides a prototypical example to demonstrate the prowess of PEPICO spectroscopy combined with *ab initio* quantum chemical calculations and statistical thermodynamics. Using these methods, we explored and characterized the six fragmentation channels with confidence, providing encouraging results indicating that the same approach can be extended to other complicated systems in future studies of gas phase ion chemistry of small organic molecules. In a broader context, this challenging mechanism may help validate automated reaction discovery and mass spectra prediction methods.

Acknowledgements

19

References

[1]   K. Voronova; C. M. M. Easter; K. G. Torma; A. Bodi; P. Hemberger; B. Sztáray, Bifurcated dissociative photoionization mechanism of acetic acid anhydride revealed by imaging photoelectron photoion coincidence spectroscopy. *Phys. Chem. Chem. Phys.* **2016,** *18*(36), 25161.

[2]   X. Wu; X. Zhou; P. Hemberger; A. Bodi, Dissociative photoionization of dimethyl carbonate: The more it is cut, the bigger the fragment ion. *J. Phys. Chem. A* **2017,** *121*(14), 2748.

[3]   B. Sztáray; A. Bodi; T. Baer, Modeling unimolecular reactions in photoelectron photoion coincidence experiments. *J. Mass Spectrom.* **2010,** *45*(11), 1233.

[4]   M. Winfough; K. Voronova; G. Muller; G. Laguisma; B. Sztáray; A. Bodi; G. Meloni, Furfural: The unimolecular dissociative photoionization mechanism of the simplest furanic aldehyde. *J. Phys. Chem. A* **2017,** *121*(18), 3401.

[5]   M. F. Heringa; J. G. Slowik; A. S. Prévôt; U. Baltensperger; P. Hemberger; A. Bodi, Dissociative ionization mechanism and appearance energies in adipic acid revealed by imaging photoelectron photoion coincidence, selective deuteration, and calculations. *J. Phys. Chem. A* **2016,** *120*(20), 3397.

[6]   K. G. Torma; K. Voronova; B. Sztaray; A. Bodi, Dissociative photoionization of the C_7H_8 isomers cycloheptatriene and toluene: Looking at two sides of the same coin simultaneously. *J. Phys. Chem. A* **2019**.

[7]   V. Ásgeirsson; C. A. Bauer; S. Grimme, Quantum chemical calculation of electron ionization mass spectra for general organic and inorganic molecules. *Chem. Sci.* **2017,** *8*(7), 4879.

[8]   S. Grimme, Towards first principles calculation of electron impact mass spectra of molecules. *Angew. Chem. Int. Ed.* **2013,** *52*(24), 6306.

[9]   C. A. Grambow; A. Jamal; Y.-P. Li; W. H. Green; J. Zador; Y. V. Suleimanov, Unimolecular reaction pathways of a γ-ketohydroperoxide from combined application of automated reaction discovery methods. *J. Am. Chem. Soc.* **2018,** *140*(3), 1035.

[10]   C. A. Bauer; S. Grimme, Automated quantum chemistry based molecular dynamics simulations of electron ionization induced fragmentations of the nucleobases uracil, thymine, cytosine, and guanine. *Eur. J. Mass Spectrom.* **2015,** *21*(3), 125.

[11]   S. Liang; P. Hemberger; N. M. Neisius; A. Bodi; H. Grützmacher; J. Levalois-Grützmacher; S. Gaan, Elucidating the thermal decomposition of dimethyl methylphosphonate by vacuum ultraviolet (VUV) photoionization: Pathways to the PO radical, a key species in flame-retardant mechanisms. *Chem.: Eur. J.* **2015,** *21*(3), 1073.

[12]   M. Okada; Y. Yamashita; Y. Ishii, Polymerization of 1,3-dioxolane. *Macromol. Chem. Phys.* **1964,** *80*(1), 196.

[13]   L. C. Reibel; C. P. Durand; E. Franta, Cationic polymerization of 1,3-dioxolane and 1,3-dioxepane. Application to graft and block copolymer synthesis. *Can. J. Chem.* **1985,** *63*(1), 264.

20

[14]   J. M. Williams; H.-R. Schulten; N. E. Vanderborgh; R. D. Walker, Polymerization-depolymerization of 1,3-dioxolane. *Polymer* **1992,** *33*(21), 4630.

[15]   W. Liu; F. Mikeš; Y. Guo; Y. Koike; Y. Okamoto, Free-radical polymerization of dioxolane and dioxane derivatives: Effect of fluorine substituents on the ring opening polymerization. *J. Polym. Sci., Part A: Polym. Chem.* **2004,** *42*(20), 5180.

[16]   J. Song; V. Zello; A. L. Boehman; F. J. Waller, Comparison of the impact of intake oxygen enrichment and fuel oxygenation on diesel combustion and emissions. *Energy & Fuels* **2004,** *18*(5), 1282.

[17]   E. Garcia; M. Laca; E. Pérez; A. Garrido; J. Peinado, New class of acetal derived from glycerin as a biodiesel fuel component. *Energy & Fuels* **2008,** *22*(6), 4274.

[18]   B. L. Wegenhart; M. M. Abu-Omar, A solvent-free method for making dioxolane and dioxane from the biorenewables glycerol and furfural catalyzed by oxorhenium (V) oxazoline. *Inorg. Chem.* **2010,** *49*(11), 4741.

[19]   V. Vol'eva; I. Belostotskaya; N. Komissarova; E. Koverzanova; L. Kurkovskaya; R. Usmanov; F. Gumerov, Synthesis of biodiesel without formation of free glycerol. *Russ. J. Org. Chem.* **2015,** *51*(7), 915.

[20]   J. Holmes; J. Turlouw; F. Lossing, The thermochemistry of $C_2H_4O^+$ ions. *J. Phys. Chem.* **1976,** *80*(26), 2860.

[21]   G. Conde-Caprace; J. Collin, Ionization and dissociation of cyclic ethers and thioethers by electron-impact. A comparison between 1,3-dioxolane, 1,3-dithiolane and 1,3-oxathiolane. *J. Mass Spectrom.* **1972,** *6*(4), 415.

[22]   M. Johnson; A. Bodi; L. Schulz; T. Gerber, Vacuum ultraviolet beamline at the swiss light source for chemical dynamics studies. *Nucl. Instrum. Methods Phys. Res. A* **2009,** *610*(2), 597.

[23]   B. Sztáray; K. Voronova; K. G. Torma; K. J. Covert; A. Bodi; P. Hemberger; T. Gerber; D. L. Osborn, CRF-PEPICO: Double velocity map imaging photoelectron photoion coincidence spectroscopy for reaction kinetics studies. *J. Phys. Chem.* **2017,** *147*(1), 013944.

[24]   A. Bodi; B. Sztáray; T. Baer; M. Johnson; T. Gerber, Data acquisition schemes for continuous two-particle time-of-flight coincidence experiments. *Rev. Sci. Instrum.* **2007,** *78*(8), 084102.

[25]   B. Sztáray; T. Baer, Suppression of hot electrons in threshold photoelectron photoion coincidence spectroscopy using velocity focusing optics. *Rev. Sci. Instrum.* **2003,** *74*(8), 3763.

[26]   W. Wiley; I. H. McLaren, Time-of-flight mass spectrometer with improved resolution. *Rev. Sci. Instrum.* **1955,** *26*(12), 1150.

[27]   B. West; C. Joblin; V. Blanchet; A. Bodi; B. l. Sztáray; P. M. Mayer, On the dissociation of the naphthalene radical cation: New iPEPICO and tandem mass spectrometry results. *J. Phys. Chem. A* **2012,** *116*(45), 10999.

[28]   J. Bouwman; B. l. Sztáray; J. Oomens; P. Hemberger; A. Bodi, Dissociative photoionization of quinoline and isoquinoline. *J. Phys. Chem. A* **2015,** *119*(7), 1127.

[29]   M. Frisch; G. Trucks; H. Schlegel; G. Scuseria; M. Robb; J. Cheeseman; G. Scalmani; V. Barone; B. Mennucci; G. Petersson, Gaussian 09, Revision A. 2. **2009**.

[30]   C. Peng; H. Bernhard Schlegel, Combining synchronous transit and quasi-newton methods to find transition states. *Isr. J. Chem.* **1993,** *33*(4), 449.

[31]   C. Peng; P. Y. Ayala; H. B. Schlegel; M. J. Frisch, Using redundant internal coordinates to optimize equilibrium geometries and transition states. *J. Comput. Chem.* **1996,** *17*(1), 49.

[32]   A. D. Becke, A new mixing of Hartree–Fock and local density-functional theories. *J. Phys. Chem.* **1993,** *98*(2), 1372.

[33]   C. Lee; W. Yang; R. G. Parr, Development of the Colle-Salvetti correlation-energy formula into a functional of the electron density. *Phys. Rev. B* **1988,** *37*(2), 785.

[34]   C. E. Klots, Kinetic energy distributions from unimolecular decay: Predictions of the Langevin model. *J. Phys. Chem.* **1976,** *64*(11), 4269.

[35]   K. Fukui, The path of chemical reactions-the IRC approach. *Acc. Chem. Res.* **1981,** *14*(12), 363.

[36]   L. A. Curtiss; P. C. Redfern; K. Raghavachari, Gaussian-4 theory. *J. Phys. Chem.* **2007,** *126*(8), 084108.

[37]   J. A. Montgomery Jr; M. J. Frisch; J. W. Ochterski; G. A. Petersson, A complete basis set model chemistry. VI. Use of density functional geometries and frequencies. *J. Phys. Chem.* **1999,** *110*(6), 2822.

[38]   A. G. Baboul; L. A. Curtiss; P. C. Redfern; K. Raghavachari, Gaussian-3 theory using density functional geometries and zero-point energies. *J. Phys. Chem.* **1999,** *110*(16), 7650.

[39]   E. C. Barnes; G. A. Petersson; J. A. Montgomery Jr; M. J. Frisch; J. M. Martin, Unrestricted coupled cluster and brueckner doubles variations of W1 theory. *J. Chem. Theory Comput.* **2009,** *5*(10), 2687.

[40]   A. Bodi; P. Hemberger; R. P. Tuckett, Coincident velocity map image reconstruction illustrated by the single-photon valence photoionisation of CF_3SF_5. *Phys. Chem. Chem. Phys.* **2017,** *19*(44), 30173.

[41]   S. Borkar; B. Sztáray; A. Bodi, Dissociative photoionization mechanism of methanol isotopologues (CH_3OH, CD_3OH, CH_3OD and CD_3OD) by iPEPICO: Energetics, statistical and non-statistical kinetics and isotope effects. *Phys. Chem. Chem. Phys.* **2011,** *13*(28), 13009.

[42]   J. Harvey; A. Bodi; R. P. Tuckett; B. Sztáray, Dissociation dynamics of fluorinated ethene cations: From time bombs on a molecular level to double-regime dissociators. *Phys. Chem. Chem. Phys.* **2012,** *14*(11), 3935.

[43]   K. Voronova; K. G. Torma; J. P. Kercher; A. Bodi; B. Sztáray, Dissociative photoionization of chromium hexacarbonyl: A round-trip ticket to non-statisticality and a detective story in thermochemistry. *Int. J. Mass spectrom.* **2019,** *438*, 63.

[44]   B. Ruscic, Uncertainty quantification in thermochemistry, benchmarking electronic structure computations, and active thermochemical tables. *Int. J. Quantum Chem.* **2014,** *114*(17), 1097.

[45]   O. K. Rice; H. C. Ramsperger, Theories of unimolecular gas reactions at low pressures. *J. Am. Chem. Soc.* **1927,** *49*(7), 1617.

[46]   O. K. Rice; H. C. Ramsperger, Theories of unimolecular gas reactions at low pressures. II. *J. Am. Chem. Soc.* **1928,** *50*(3), 617.

[47]   R. A. Marcus; O. Rice, The kinetics of the recombination of methyl radicals and iodine atoms. *J. Phys. Chem.* **1951,** *55*(6), 894.

[48]   T. Beyer; D. Swinehart, Algorithm 448: Number of multiply-restricted partitions. *Commun. ACM* **1973,** *16*(6), 379.

[49]   K. Voronova; C. M. Mozaffari Easter; K. J. Covert; A. Bodi; P. Hemberger; B. Sztáray, Dissociative photoionization of diethyl ether. *J. Phys. Chem. A* **2015,** *119*(43), 10654.

[50]   J. Collin; G. Conde, Spectrometrie de masse-l'ionisation et la dissociation des polyethers cycliques soumis a l'impact electronique. *Bull. Acad. R. Belg.* **1966,** *52*(7), 978.

[51]   D. Sweigart; D. Turner, Lone pair orbitals and their interactions studied by photoelectron spectroscopy. II. Equivalent orbitals in saturated oxygen and sulfur heterocycles. *J. Am. Chem. Soc.* **1972,** *94*(16), 5599.

[52]   P. Hemberger; A. Bodi; T. Gerber; M. Würtemberger; U. Radius, Unimolecular reaction mechanism of an imidazolin-2-ylidene: An iPEPICO study on the complex dissociation of an Arduengo-type carbene. *Chem. Eur. J.* **2013,** *19*(22), 7090.

[53]   T. Baer; W. L. Hase, *Unimolecular reaction dynamics: Theory and experiments*. Oxford University Press: New York, 1996.

[54]   A. Bodi; M. D. Brannock; B. Sztáray; T. Baer, Tunneling in H loss from energy selected ethanol ions. *Phys. Chem. Chem. Phys.* **2012,** *14*(46), 16047.

[55]   A. de Saint-Exupéry, *Le petit prince*. Gallimard: 1999.

[56]   F. Dyson, A meeting with Enrico Fermi. *Nature* **2004,** *427*(6972), 297.

[57]   W. J. Bouma; J. K. MacLeod; L. Radom, An ab initio molecular orbital study of the structures and stabilities of the $C_2H_4O^+$ Isomers. *J. Am. Chem. Soc.* **1979,** *101*(19), 5540.

22

[58]   B. C. Baumann; J. K. MacLeod, Structures of the $C_2H_4O^+$ gas-phase isomers. Evidence for the formation of the $CH_2OCH_2^+$ ion from ethylene carbonate. *J. Am. Chem. Soc.* **1981,** *103*(20), 6223.

[59]   R. Bombach; J.-P. Stadelmann; J. Vogt, The fragmentation and isomerization of internal energy selected acetaldehyde molecular cations. *Chem. Phys.* **1981,** *60*(3), 293.

[60]   R. Krässig; D. Reinke; H. Baumgärtel, Photoreaktionen kleiner organischer moleküle II. Die photoionenspektren der isomeren propylen-cyclopropan und acetaldehyd-äthylenoxyd. *Ber. Bunsenges. Phys. Chem.* **1974,** *78*(5), 425.

[61]   P. C. Burgers; J. L. Holmes, Metastable ion studies: XIII—the measurement of appearance energies of metastable peaks. *Org. Mass Spectrom.* **1982,** *17*(3), 123.
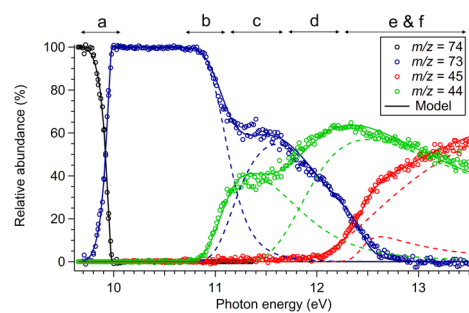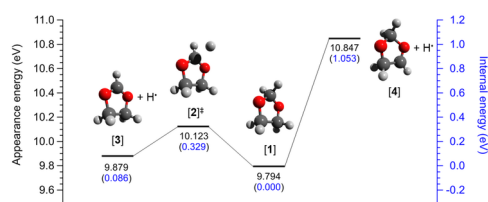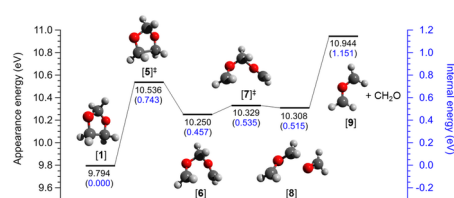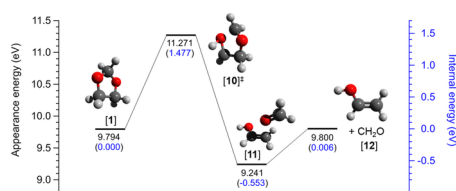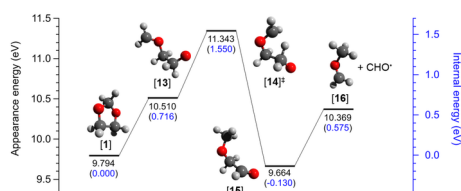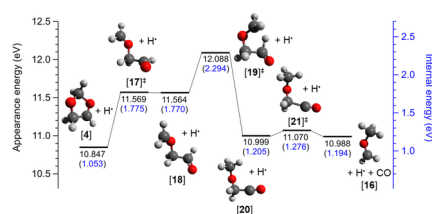
JMS_4522_F1.tif
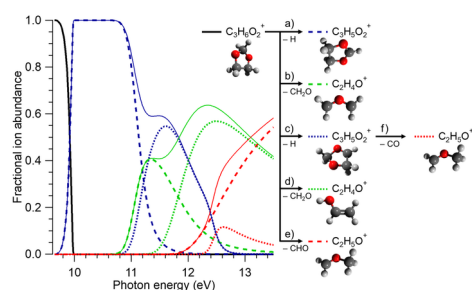
JMS_4522_F2.tif

JMS_4522_F3.tif

JMS_4522_F4.TIF

JMS_4522_F5.TIF

JMS_4522_F6.TIF

JMS_4522_F7.TIF